Inorganic Chemistry

ARTICLE

pubs.acs.org/IC

Synthesis, Structural Analysis, and Magnetic Properties of Ethylmalonate-Manganese(II) Complexes

Mariadel Déniz,[†] Jorge Pasán,[*,†] Jesús Ferrando-Soria,[‡] Oscar Fabelo,[†,⊥] Laura Cañadillas-Delgado,[†,⊥] Consuelo Yuste,[‡] Miguel Julve,[‡] Joan Cano,[‡,§] and Catalina Ruiz-Pérez[*,†]

[†]Laboratorio de Rayos X y Materiales Moleculares (MATMOL), Departamento de Física Fundamental II, Facultad de Física, Universidad de La Laguna, Avenida Astrofísico Francisco Sánchez s/n, E-38204 La Laguna, Tenerife, Spain

[‡]Departament de Química Inorgànica, Instituto de Ciencia Molecular (ICMol), Universitat de València, C/Catedrático José Beltrán no. 2, 46980 Paterna, Valencia, Spain

[§]Fundació General de la Universitat de València (FGUV), Universitat de València, Valencia, Spain

Supporting Information

ABSTRACT: Five manganese(II) complexes of formulas $[Mn_2(Etmal)_2(H_2O)_2(L)]_n$ (**1**−**4**) and $\{[Mn(Etmal)_2(H_2O)][Mn(H_2O)_4]\}_n$ (**5**) with H_2Etmal = ethylmalonic acid (**1**−**5**) and L = 1,2-bis(4-pyridyl)ethane (bpa) (**1**), 4,4′-azobispyridine (azpy) (**2**), 4,4′-bipyridyl (4,4′-bpy) (**3**), and 1,2-bis(4-pyridyl)ethylene (bpe) (**4**) were synthesized and structurally characterized by single crystal X-ray diffraction. Their thermal behavior and variable-temperature magnetic properties were also investigated. The structure of the compounds **1**−**4** consists of corrugated layers of aquamanganese(II) units with intralayer carboxylate-ethylmalonate bridges in the *anti-syn* (equatorial-equatorial) coordination mode which are linked through bis-monodentate bpa (**1**), azpy (**2**), 4,4′-bpy (**3**), and bpe (**4**) ligands to build up a three-dimensional (3D) framework. The structure of compound **5** is made up by zigzag chains of manganese(II) ions with a regular alternation of $[Mn(H_2O)_4]^{2+}$ and chiral (either Δ or λ enantiomeric forms) $[Mn(Etmal)_2(H_2O)]^{2-}$ units within each chain. In contrast to the bidentate/bis-monodentate coordination mode of the Etmal ligand in **1**−**4**, it adopts the bidentate/monodentate coordination mode in **5** with the bridging carboxylate-ethylmalonate also exhibiting the *anti-syn* conformation but connecting one equatorial and an axial position from adjacent metal centers. The manganese−manganese separation through the carboxylate-ethylmalonate bridge in **1**−**5** vary in the range 5.3167(4)−5.5336(7) Å. These values are much shorter than those across the extended bis-monodentate N-donors in **1**−**4** with longest/shortest values of 11.682(3) (**3**)/13.9745(9) Å (**4**). Compounds **1**−**5** exhibit an overall antiferromagnetic behavior, where the exchange pathway is provided by the carboxylate-ethylmalonate bridge. Monte Carlo simulations based on the classical spin approach (**1**−**5**) were used to successfully reproduce the magnetic data of **1**−**5**.

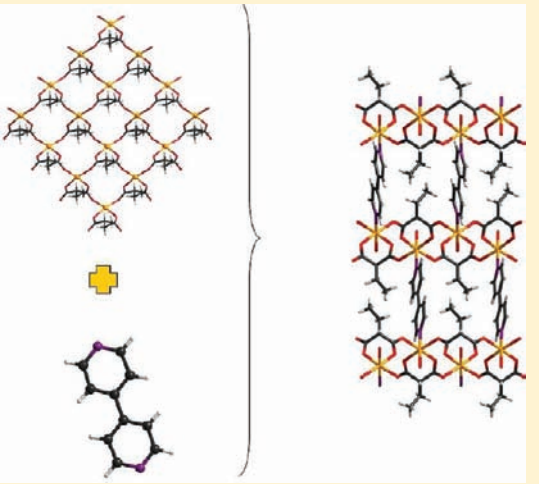

INTRODUCTION

Carboxylate-containing organic molecules are frequently used as bridging ligands in the design of polynuclear complexes which exhibit interesting magnetic properties.[1] The ability of the carboxylate to mediate significant ferro- or antiferromagnetic interactions between the magnetic centers that it links accounts for their thorough use in magneto-chemistry.[2] Among the dicarboxylate ligands, the dianion of malonic acid (H_2mal) has been one of the more widely used because of its richness and variety of coordination modes.[3] The malonate group fills two coordination positions at the metal ion when acting as a bidentate ligand forming a very stable six-membered chelate ring, and in addition, it can use its free carboxylate-oxygens as donors adopting the *syn-syn*, *syn-anti*, and *anti-anti* bridging modes. These coordination modes allow the inclusion of other groups (the so-called coligands or auxiliary ligands) in the coordination sphere of the cation, that in turn act as bridging or blocking ligands contributing to the interconnection or isolation of the spin carriers and eventually to achieve the electroneutrality of the resulting motif.[4] This synthetic strategy which consists of combining the malonate with other bridging and/or blocking ligands has afforded a good number of compounds of variable dimensionality (nD systems with n = 0−3).[3,5]

Systematic studies concerning the complex formation between copper(II) and substituted malonate ligands, where one of the two hydrogen atoms of the methylene carbon atom is replaced by an alkyl or aryl substituent have been undertaken

Received: June 18, 2011
Published: October 10, 2011

Table 1. Crystallographic Data for Complexes 1−5

	1	2	3	4	5
formula	$C_{11}H_{14}MnNO_5$	$C_{10}H_{12}MnN_2O_5$	$C_{10}H_{12}MnNO_5$	$C_{11}H_{13}MnNO_5$	$C_{10}H_{22}Mn_2O_{13}$
FW	295.17	295.16	281.15	294.16	460.16
crystal system	monoclinic	monoclinic	monoclinic	monoclinic	orthorhombic
space group	$P2_1/n$	$P2_1/n$	$P2_1/n$	$P2_1/n$	$C222_1$
a (Å)	7.2800(15)	7.2812(11)	7.4309(6)	7.3025(6)	10.4333(10)
b (Å)	23.943(5)	23.446(3)	21.370(5)	23.7239(18)	12.167(2)
c (Å)	7.6140(15)	7.6503(7)	7.4721(10)	7.6867(6)	13.8077(11)
β (deg)	90.8(3)	91.680(9)	90.357(9)	91.548(7)	
V (Å^3)	1327.2(5)	1305.5(3)	1186.6(3)	1331.19(18)	1752.8(4)
Z	4	4	4	4	4
μ (Mo Kα)(cm^{-1})	1.006	1.025	1.121	1.003	1.504
T (K)	100(2)	293(2)	293(2)	293(2)	293(2)
ρ_{calc} (g cm^{-3})	1.477	1.502	1.574	1.468	1.744
λ (Å)	0.72950	0.71073	0.71073	0.71073	0.71073
index ranges	$-10 \le h \le 9$	$-8 \le h \le 9$	$-9 \le h \le 8$	$-9 \le h \le 9$	$-13 \le h \le 13$
	$-32 \le k \le 32$	$-27 \le k \le 30$	$-25 \le k \le 27$	$-27 \le k \le 30$	$-15 \le k \le 15$
	$-10 \le l \le 9$	$-9 \le l \le 5$	$-9 \le l \le 8$	$-9 \le l \le 9$	$-17 \le l \le 17$
indep. reflect. (R_{int})	3387 (0.0374)	2940 (0.0473)	2656 (0.0454)	3028 (0.0381)	2020 (0.0188)
Flack parameter					0.477(10)
obs. reflect. [$I > 2\sigma(I)$]	3363	1860	2065	2290	1956
parameters	171	171	154	175	160
goodness-of-fit	1.263	1.094	1.197	1.127	1.124
R [$I > 2\sigma(I)$]	0.0870	0.0644	0.1113	0.0447	0.0142
R_w [$I > 2\sigma(I)$]	0.2231	0.1083	0.2818	0.0817	0.0340
R (all data)	0.0882	0.1207	0.1353	0.0711	0.0156
R_w (all data)	0.2258	0.1239	0.2926	0.0897	0.0346

having in mind that subtle modifications of the malonate group could be a useful tool to exert some control over the intermolecular interactions and then, to an added value when thinking of the structural and physical properties of these malonate complexes.[6,7] Several points are important when looking at this strategy concerning the alkyl/aryl-substituted malonate, the main ones being the control of the solubility in polar and non polar solvents, the hydrophobic character, the electron donor or acceptor effects, and the possibility of additional intermolecular interactions ($\pi-\pi$ stacking) and new conformation/coordination modes of the substituted malonate. As far as the hydrophobic effects are concerned, they are certainly relevant when thinking of the host−guest chemistry with open frameworks based on malonate complexes.

Herein we report the synthesis, structural characterization, and thermal and magnetic investigation of five new manganese(II) complexes of formulas $[Mn_2(Etmal)_2(H_2O)_2(L)]_n$ (**1**−**4**) and $\{[Mn(Etmal)_2(H_2O)][Mn(H_2O)_4]\}_n$ (**5**) with H_2Etmal = ethylmalonic acid (**1**−**5**) and L = 1,2-bis(4-pyridyl)ethane (bpa) (**1**), 4,4′-azobispyridine (azpy) (**2**), 4,4′-bipyridyl (4,4′-bpy) (**3**), and 1,2-bis(4-pyridyl)ethylene (bpe) (**4**).

EXPERIMENTAL SECTION

Materials. H_2Etmal, $MnCl_2\cdot 4H_2O$, Na_2CO_3, 4,4′-bpy, bpa, bpe, and ethanol were purchased from commercial sources and used without further purification. The azpy ligand was synthesized by means of the oxidation of 4-aminopyridine by a solution of sodium hypochlorite.[8] Elemental analyses (C, H, and N) were performed on an EA 1108 CHNS-O microanalytical analyzer of the SEGAI service of the University of Laguna (Tenerife).

Synthesis of $[Mn_2(Etmal)_2(H_2O)_2(L)]_n$ with L = bpa (1) and azpy (2), 4,4′-bpy (3) and bpe (4). Complexes **1**−**4** were obtained by the reaction of stoichiometric amounts of the manganese(II)-ethylmalonate with the corresponding N-donor in mixed water−ethanol solutions. The detailed procedure is as follows: a mixture of ethylmalonic acid (0.5 mmol, 66 mg) and sodium carbonate (0.5 mmol, 53 mg) in water (5 cm^3) was added to an aqueous solution (3 cm^3) of manganese(II) chloride tetrahydrate (0.5 mmol, 99 mg). The resulting colorless clear solution was placed at the bottom of a test tube and then, a water interphase (10 cm^3) was added dropwise. Finally, an ethanolic solution (4 cm^3) of bpa (0.5 mmol, 92 mg) (**1**), azpy (0.5 mmol, 92 mg) (**2**), 4,4′-bpy (0.5 mmol, 78 mg) (**3**), or bpe (0.5 mmol, 91 mg) (**4**) was carefully layered on the water interphase. The tube was covered with parafilm and left at room temperature. Suitable crystals for X-ray diffraction as colorless (**1** and **3**), orange (**2**), and yellow prisms (**4**) were grown in the interphase after a few days. Yield about 82 (**1**), 87 (**2**), 83 (**3**), and 89% (**4**). Anal. Calcd for $C_{22}H_{28}Mn_2N_2O_{10}$ (**1**): C, 44.78; H, 4.74; N, 4.74. Found: C, 44.61; H, 4.65; N 4.63%. Anal. Calcd for $C_{20}H_{24}Mn_2N_4O_{10}$ (**2**): C, 40.71; H, 4.07; N, 9.49. Found: C, 40.59; H, 3.96; N 9.40%. Anal. Calcd for $C_{20}H_{24}Mn_2N_2O_{10}$ (**3**): C, 42.73; H, 4.27; N, 4.98. Found: C, 42.56; H, 4.19; N, 4.85%. Anal. Calcd for $C_{22}H_{26}MnN_2O_{10}$ (**4**): C, 44.93; H, 4.42; N, 4.76. Found: C, 44.74; H, 4.33; N, 4.65%. Selected IR peaks (KBr, cm^{-1}): 3258 w, 1559vs, 1426 m, 1332 m, 692s, 595 m (**1**); 3256w, 1561vs, 1432 m, 1332 m, 689s, 601 m (**2**); 3268w, 1558vs, 1429 m, 1332s, 689s, 623s (**3**); 3252w, 1558vs, 1425 m, 1332s, 691s, 547s (**4**).

Synthesis of $\{[Mn(Etmal)_2(H_2O)][Mn(H_2O)_4]\}_n$ (5). An ethanolic solution (5 cm^3) of manganese(II) chloride tetrahydrate

dx.doi.org/10.1021/ic201314k |*Inorg. Chem.* 2011, 50, 10765–10776

Table 2. Selected Bond Length (Å) and Angles (deg) for 1−4[a]

			1		
Mn(1)−O(2)	2.153(3)	O(3d)−Mn(1)−O(4)	172.22(14)	O(4)−Mn(1)−O(1W)	92.05(13)
Mn(1)−O(4)	2.162(3)	O(2)−Mn(1)−O(4)	83.60(13)	O(1c)−Mn(1)−O(1W)	91.85(13)
Mn(1)−O(1c)	2.162(3)	O(3d)−Mn(1)−O(1c)	96.93(14)	O(3d)−Mn(1)−N(1)	87.19(14)
Mn(1)−O(3d)	2.157(3)	O(2)−Mn(1)−O(1c)	170.99(14)	O(2)−Mn(1)−N(1)	88.58(14)
Mn(1)−O(1W)	2.223(3)	O(4)−Mn(1)−O(1c)	89.86(13)	O(4)−Mn(1)−N(1)	89.62(15)
Mn(1)−N(1)	2.261(4)	O(3d)−Mn(1)−O(1W)	91.52(13)	O(1c)−Mn(1)−N(1)	85.17(14)
O(3d)−Mn(1)−O(2)	89.23(13)	O(2)−Mn(1)−O(1W)	94.56(13)	O(1W)−Mn(1)−N(1)	176.59(14)
			2		
Mn(1)−O(2)	2.151(3)	O(3d)−Mn(1)−O(4)	171.85(12)	O(4)−Mn(1)−O(1W)	91.33(12)
Mn(1)−O(4)	2.154(3)	O(2)−Mn(1)−O(4)	83.35(11)	O(1c)−Mn(1)−O(1W)	91.07(12)
Mn(1)−O(1c)	2.161(3)	O(3d)−Mn(1)−O(1c)	97.88(12)	O(3d)−Mn(1)−N(1)	87.57(13)
Mn(1)−O(3d)	2.149(3)	O(2)−Mn(1)−O(1c)	170.09(12)	O(2)−Mn(1)−N(1)	88.91(13)
Mn(1)−O(1W)	2.229(3)	O(4)−Mn(1)−O(1c)	89.05(12)	O(4)−Mn(1)−N(1)	88.82(13)
Mn(1)−N(1)	2.296(4)	O(3d)−Mn(1)−O(1W)	92.82(12)	O(1c)−Mn(1)−N(1)	84.57(13)
O(3d)−Mn(1)−O(2)	89.27(12)	O(2)−Mn(1)−O(1W)	95.45(12)	O(1W)−Mn(1)−N(1)	175.63(13)
			3		
Mn(1)−O(2)	2.182(7)	O(3d)−Mn(1)−O(4)	169.9(3)	O(4)−Mn(1)−O(1W)	93.5(3)
Mn(1)−O(4)	2.149(7)	O(2)−Mn(1)−O(4)	82.5(3)	O(1a)−Mn(1)−O(1W)	90.8(3)
Mn(1)−O(1a)	2.150(7)	O(3d)−Mn(1)−O(1a)	99.6(3)	O(3d)−Mn(1)−N(1)	85.9(3)
Mn(1)−O(3d)	2.156(7)	O(2)−Mn(1)−O(1a)	171.2(3)	O(2)−Mn(1)−N(1)	91.0(3)
Mn(1)−O(1W)	2.229(7)	O(4)−Mn(1)−O(1a)	89.1(3)	O(4)−Mn(1)−N(1)	89.7(3)
Mn(1)−N(1)	2.290(8)	O(3d)−Mn(1)−O(1W)	91.5(3)	O(1a)−Mn(1)−N(1)	86.2(3)
O(3d)−Mn(1)−O(2)	88.5(3)	O(2)−Mn(1)−O(1W)	92.3(3)	O(1W)−Mn(1)−N(1)	175.7(3)
			4		
Mn(1)−O(2)	2.1572(18)	O(3d)−Mn(1)−O(4)	171.66(7)	O(4)−Mn(1)−O(1W)	91.31(7)
Mn(1)−O(4)	2.1605(18)	O(2)−Mn(1)−O(4)	83.01(7)	O(1c)−Mn(1)−O(1W)	90.03(7)
Mn(1)−O(1c)	2.1662(18)	O(3d)−Mn(1)−O(1c)	97.83(8)	O(3d)−Mn(1)−N(1)	88.80(8)
Mn(1)−O(3d)	2.1523(18)	O(2)−Mn(1)−O(1c)	170.71(7)	O(2)−Mn(1)−N(1)	89.17(8)
Mn(1)−O(1W)	2.2312(19)	O(4)−Mn(1)−O(1c)	89.68(7)	O(4)−Mn(1)−N(1)	88.26(8)
Mn(1)−N(1)	2.289(2)	O(3d)−Mn(1)−O(1W)	92.31(7)	O(1c)−Mn(1)−N(1)	84.87(8)
O(3d)−Mn(1)−O(2)	89.14(7)	O(2)−Mn(1)−O(1W)	95.85(7)	O(1W)−Mn(1)−N(1)	174.88(8)

[a] Symmetry code: (a) = $x-1/2, -y+1/2, z+1/2$; (c) = $x+1/2, -y+1/2, z-1/2$; (d) = $x-1/2, -y+1/2, z-1/2$.

(0.5 mmol, 99 mg) was added to an aqueous solution (5 cm^3) of ethylmalonic acid (0.5 mmol, 66 mg) and sodium carbonate (0.5 mmol, 53 mg) under continuous stirring. The resulting colorless solution was filtered and allowed to evaporate at room temperature. X-ray quality crystals as colorless prisms were grown after 1 day. They were filtered, washed with small amounts of water and ethanol, and dried on filter paper. Yield about 87%. Anal. Calcd for $C_{10}H_{22}Mn_2O_{13}$ (**5**): C, 26.11; H, 4.78. Found: C, 26.03; H, 4.59. Selected IR peaks (KBr, cm^{-1}): 3308 m, 1558vs, 1424 m, 1349s, 669s, 595s.

Physical Techniques. IR spectra (450−4000 cm^{-1}) were recorded on a Bruker IF S66 spectrophotometer with an ATR module for solid samples over the range 4000−500 cm^{-1}. The thermogravimetric analyses were performed on a Perkin-Elmer Pyris Diamond, TGA/DTA equipment. Samples were heated in Al_2O_3 crucibles from 40 to 600 °C in flowing N_2 atmosphere with a heating rate of 5 °C min^{-1}. Magnetic susceptibility measurements on polycrystalline samples of compounds **1**−**5** were carried out in the temperature range 1.9−290 K with a Quantum Design SQUID magnetometer. Diamagnetic corrections of the constituent atoms were estimated from Pascal's constants[9] as -320×10^{-6} (**1**), -306×10^{-6} (**2**), -296×10^{-6} (**3**), -316×10^{-6} (**4**), and -230×10^{-6} cm^3 mol^{-1} (**5**) [per two manganese(II) ions]. Experimental susceptibilities were also corrected for the magnetization of the sample holder (a plastic bag).

X-ray Data Collection and Structure Determination. Single crystals of **2**−**5** were mounted on a Bruker-Nonius KappaCCD diffractometer, and the crystallographic data were collected at 293(2) K by using graphite-monochromated Mo−Kα radiation (λ = 0.71073 Å). Data collection of **1** was carried out in the ESRF synchrotron facilities at the BM16 beamline (Grenoble, France) with λ = 0.72950 Å at 100(2) K, and it was indexed, integrated, and scaled with the HKL2000 program.[10] The crystal structures of **1**−**5** were solved by direct methods and refined with the full-matrix least-squares technique on F^2 by using the SHELXS-97 and SHELXL-97 programs[11] included in the WINGX[12] software package. All non-hydrogen atoms were refined anisotropically. The hydrogen atoms of the organic ligands in **1**−**4** were set on geometrical positions and refined with a riding model, whereas those of **5** and of the coordinated water molecule of **1**−**4** were located from Fourier differences and refined with isotropic thermal factors. The absolute configuration of **5** could not be reliably assigned, all the crystals tested were inversion twins as the crystal used for the structure resolution [Flack parameter of 0.477(10)]. The final geometrical calculations and the graphical manipulations were carried out with the PARST95[13] and DIAMOND[14] programs. A summary of the crystallographic data and structure refinement is given in Table 1. Selected bond distances and angles for **1**−**4** and **5** are listed in Tables 2

dx.doi.org/10.1021/ic201314k |Inorg. Chem. 2011, 50, 10765–10776

Table 3. Selected Bond Length (Å) and Angles (deg) for 5[a]

Mn(1)−O(2)	2.0856(9)	Mn(2)−O(1)	2.2674(8)
Mn(1)−O(1W)	2.1016(13)	Mn(2)−O(3W)	2.1315(11)
Mn(1)−O(4)	2.1148(9)	Mn(2)−O(2W)	2.1714(10)
O(2)−Mn(1)−O(4)	86.23(4)	O(2W)−Mn(2)−O(1)	86.21(4)
O(2e)−Mn(1)−O(2)	115.63(5)	O(3W)−Mn(2)−O(1)	92.48(4)
O(2)−Mn(1)−O(1W)	122.18(3)	O(3W)−Mn(2)−O(2W)	173.35(5)
O(1W)−Mn(1)−O(4)	89.91(3)		

[a] Symmetry code: (e) = $-x, y, -z+1/2$.

Table 4. Hydrogen Bond Distances and Angles in 1−4[a,b]

D−H···A	D−H (Å)	H···A (Å)	D···A (Å)	D−H···A (deg)
		1		
O1W−H1WB···O2c	0.90(9)	1.93(9)	2.721(5)	145(8)
O1W−H1WA···O4d	0.90(12)	1.91(13)	2.733(5)	151(11)
		2		
O1W−H1WB···O2c	0.901(14)	1.92 (32)	2.791(4)	163(2)
O1W−H1WA···O4d	0.90(6)	1.91(6)	2.733(4)	150(6)
		3		
O1W···O2a			2.735(3)	
O1W···O4d			2.743(3)	
		4		
O1W−H1WB···O2c	0.88(3)	1.94(3)	2.780(3)	161(3)
O1W−H1WA···O4d	0.88(3)	1.91(3)	2.752(3)	159(3)

[a] D and A stand for donor and acceptor, respectively. [b] Symmetry code: (a) = $x-1/2, -y+1/2, z+1/2$; (c) = $x+1/2, -y+1/2, z-1/2$; (d) = $x-1/2, -y+1/2, z-1/2$.

Table 5. Hydrogen Bond Distances and Angles in 5[a,b]

D−H···A[a]	D−H (Å)	H···A (Å)	D···A (Å)	D−H···A (deg)
O1W−H1WA···O1h	0.78(2)	2.02(2)	2.789(2)	174(2)
O2W−H2WA···O3m	0.89(2)	1.81(2)	2.686(2)	172(2)
O2W−H2WB···O2f	0.77(2)	2.03(2)	2.749(2)	157(2)
O3W−H3WA···O3p	0.79(2)	1.92(2)	2.712(2)	173(2)
O3W−H3WB···O4q	0.73(2)	2.07(2)	2.791(2)	175(2)

[a] D and A stand for donor and acceptor, respectively. [b] Symmetry code: (h) = $-x+1/2, y+1/2, -z+1/2$; (m) = $-x+1/2, y-1/2, -z+1/2$; (f) = $x, -y, -z+1$; (p) = $-x+1, y, -z+1/2$; (q) = $-x+1/2, -y+1/2, z+1/2$.

and 3, respectively, whereas the hydrogen bond interactions are shown in Tables 4 (**1**−**4**) and 5 (**5**). Crystallographic data (excluding structure factors) for the structures **1**−**5** have been deposited at the Cambridge Crystallographic Data Centre with CCDC reference numbers 826328 (**1**), 826329 (**2**), 826330 (**3**), 826331 (**4**), and 826332 (**5**).

RESULTS AND DISCUSSION

Description of the Structures. *$[Mn_2(Etmal)_2(H_2O)_2(L)]_n$ with L = bpa (**1**), azpy (**2**), 4,4′-bpy (**3**), and bpe (**4**).* The crystal structures of **1**−**4** consist of neutral corrugated manganese(II)-ethylmalonate layers which are pillared through bis-monodentate bpa (**1**), azpy (**2**), 4,4′-bpy (**3**), and bpe (**4**) ligands to build

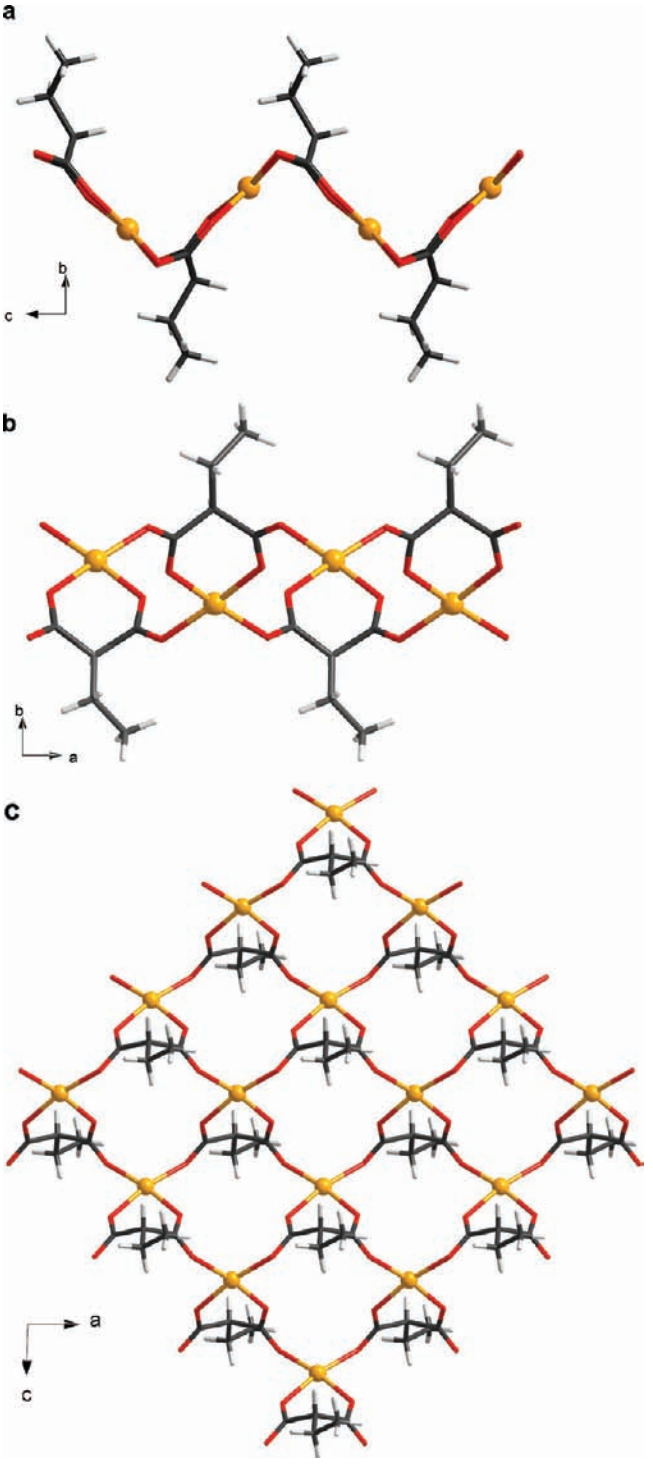

Figure 1. View of the ethylmalonate-manganese(II) layers in **1**−**4**, along the crystallographic *a* (a), *c* (b), and *b* axes (c).

up a three-dimensional (3D) network (Figures 1−3). The layers are made up of carboxylate-bridged manganese(II) ions resulting in a square grid which grows in the *ac* plane (Figures 2 and 3). The N-donor ligands are located alternatively above and below the sheets, inversely to the position of the ethyl group of the Etmal ligand. The shortest centroid-centroid distances between adjacent aromatic rings are 7.2800(15) (**1**), 7.2812(11) (**2**), 7.4721(10) (**3**), and 7.3025(6) Å (**4**), values which are much

dx.doi.org/10.1021/ic201314k |*Inorg. Chem.* 2011, 50, 10765–10776

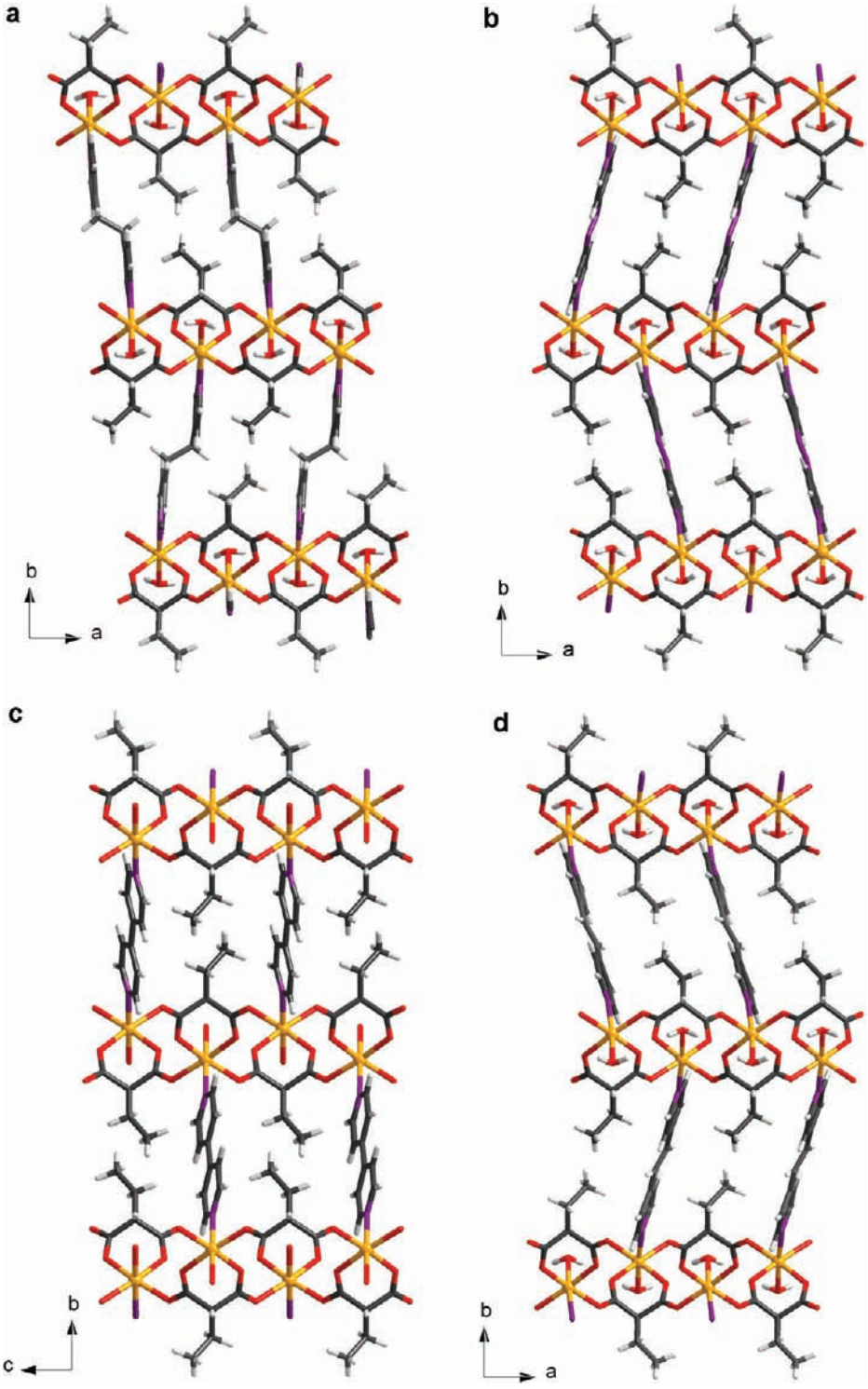

Figure 2. Perspective views of the crystal packing of **1** (a), **2** (b), **3** (c), and **4** (d) along the crystallographic *a* (**3**) and *c* axes (**1**, **2** and **4**).

longer than the average ones for any significant $\pi-\pi$ type interaction between the pyridyl rings.[15] In the same way, C−H/π intermolecular interactions are also inexistent because the values of the shortest hydrogen-centroid distances [4.1235(1) (**1**) and 4.2105(4) (**2**), 3.6839(6) (**3**) and 4.1271(2) Å (**4**)] are much longer than those observed for this type interactions between C−H and C(π).[16] Several intralayer hydrogen bonds involving the coordinated water molecule and oxygen atoms of the ethylmalonate ligand in **1**−**4** contribute to the stabilization of the structures (see Table 4).

Each manganese atom in **1**−**4** is six-coordinated with a distorted octahedral environment (see Figure 4) with the parameters *s*/*h* and ϕ being 1.250 and 58.55° (**1**), 1.257 and 58.10° (**2**), 1.257 and 58.33° (**3**), and 1.255 and 58.26° (**4**) (the values for an ideal octahedron are *s*/*h* = 1.22 and ϕ = 60°).[17] Four carboxylate-oxygen atoms build the equatorial plane [O(1),

dx.doi.org/10.1021/ic201314k |*Inorg. Chem.* 2011, 50, 10765–10776

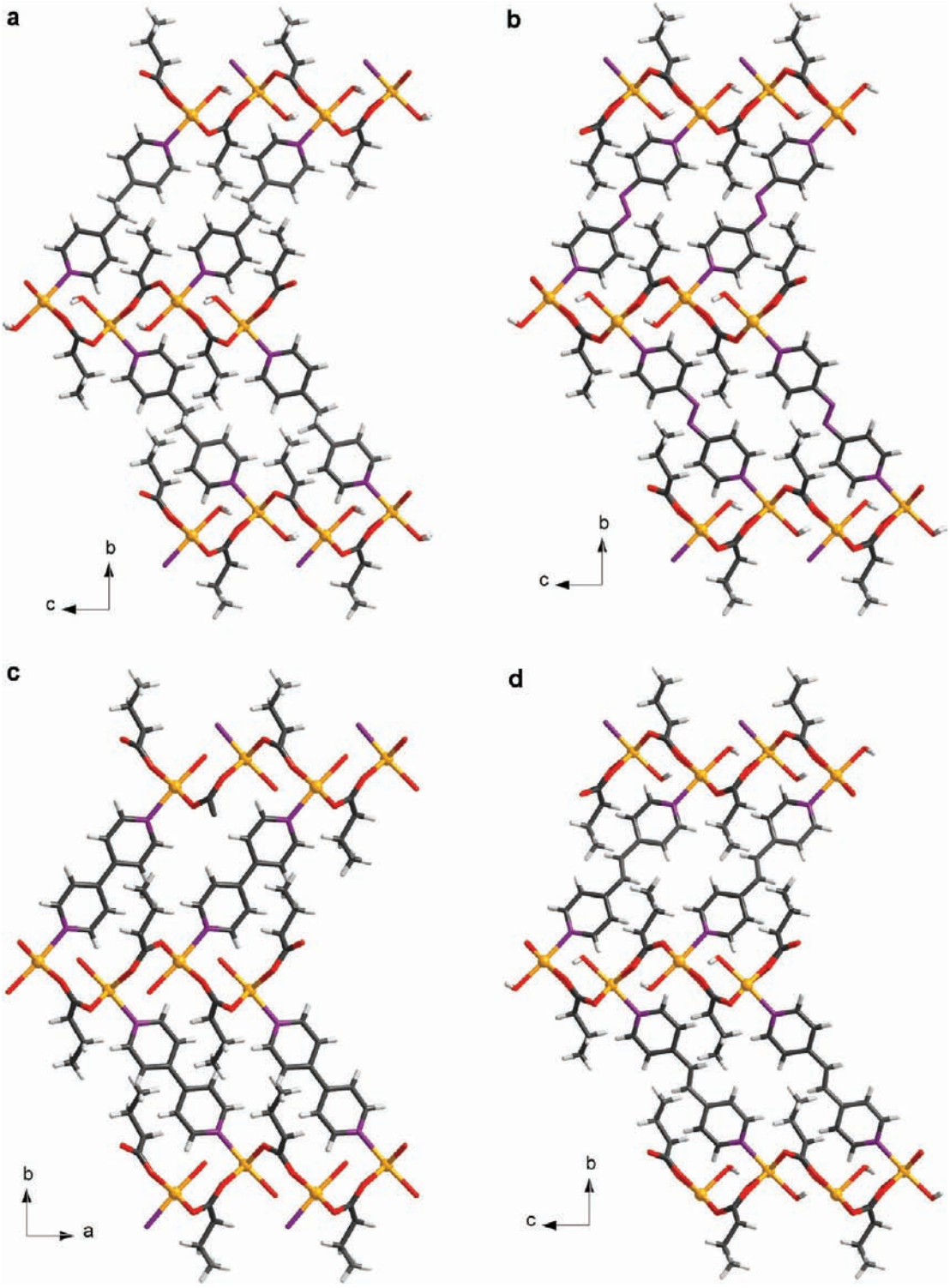

Figure 3. View of the 3D structure of the compounds **1** (a), **2** (b), **3** (c), and **4** (d) along the crystallographic *c* (**3**) and *a* axes (**1**, **2**, and **4**) showing the corrugated layers of the carboxylate-bridged manganese(II) ions linked through the respective N-donor.

O(2), O(3), and O(4) with mean values for the Mn−O(eq) bond distance of 2.159(4) (**1**), 2.154(3) (**2**), 2.159(7) (**3**), and 2.159 (2) Å (**4**)], while a nitrogen atom from the N-donor ligand [N(1)] and a coordinated water molecule [O(1W)] occupy the axial positions [average values for the axial bond lengths being 2.242(4) (**1**), 2.262(4) Å (**2**), 2.259(8) (**3**), and 2.259(2) Å (**4**)].

The ethylmalonate ligand in **1**−**4** acts simultaneously as bidentate [through O(2) and O(4) toward Mn(1) with the angle subtended at the manganese atom being 83.61(13) (**1**), 83.38(11) (**2**), 82.5(3) (**3**), and 83.01(6)° (**4**)] and as bis-monodentate ligand [through O(1) and O(3) toward Mn(1a) and Mn(1b), respectively, in case of **1**, **2**, and **4**, and toward

dx.doi.org/10.1021/ic201314k |*Inorg. Chem.* 2011, 50, 10765–10776

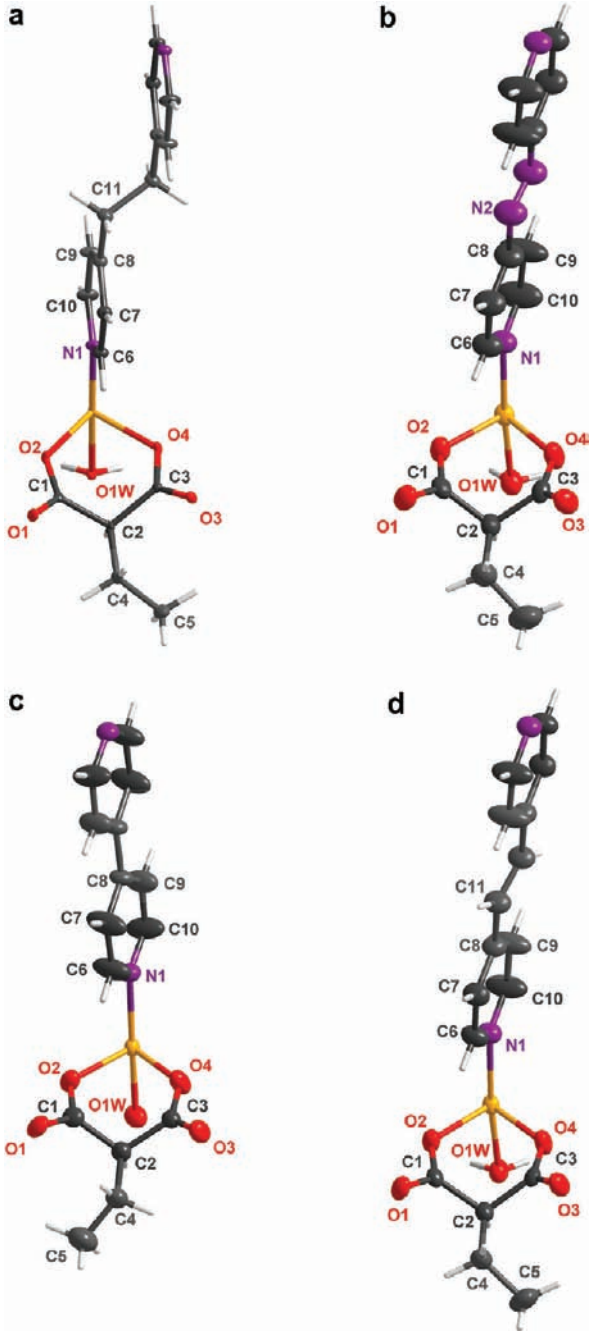

Figure 4. View of a fragment of **1** (a), **2** (b), **3** (c), and **4** (d) showing the atom numbering.

Mn(1c) and Mn(1b) in case of **3**; symmetry code: (a) = $-1/2+x$, $1/2-y$, $1/2+z$; (b) = $1/2+x$, $1/2-y$, $1/2+z$; (c) = $1/2+x$, $1/2-y$, $-1/2+z$]. The values of the manganese−manganese separation through the two *anti-syn* carboxylate bridges are 5.438(2), (**1**), 5.3668(10), (**2**), and 5.536(7) Å (**4**) [Mn(1)···Mn(1a)], 5.493(2) (**3**) [Mn(1)···Mn(1c)], and 5.445(2) (**1**), 5.5169(11) (**2**), 5.461(2) (**3**), and 5.3948(7) Å (**4**) [Mn(1)···Mn(1b)]. The carboxylate bridges link equatorial positions of adjacent manganese(II) ions in **1**−**4**. The values of the dihedral angle between the equatorial planes of neighboring Mn(II) ions for this series of compounds cover the range 86.15(13)

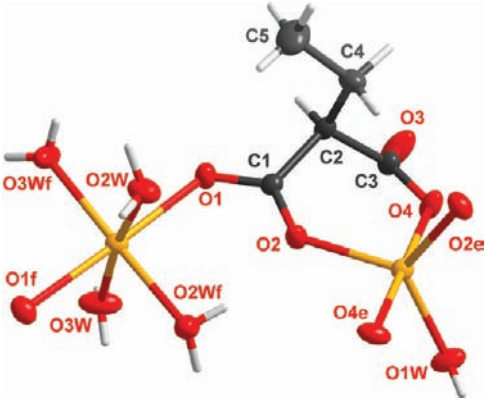

Figure 5. View of a fragment of the structure of compound **5** along with the numbering scheme.

(**3**)−88.99(5)° (**2**), being much greater than that observed in **5** between Mn(1) and Mn(2) [33.39(3)°].

The N-donor molecules in **1**−**4** act as bis-monodentate ligands connecting two manganese(II) atoms from adjacent layers, the values of the metal−metal separation across them amounting to 13.733(2) (**1**), 13.584(2) (**2**), 11.682(3) (**3**), and 13.9475(9) Å (**4**). They are somewhat longer than the shortest interlayer manganese−manganese distance [values varying in the range 9.198(3) (**3**)−10.863(2) Å (**1**)] because of the corrugation of the layers and the nonparallel alignment of the bridging ligands along the stacking direction of the layers [the values of the angle between the N-donor ligands and the normal of the layer being 36.13(3) (**1**), 35.88(2) (**2**), 34.601(10) (**3**), and 35.98(2)° (**4**)]. The pyridyl rings of the azpy (**2**), 4,4′-bpy (**3**), and bpe (**4**) molecules are coplanar, and the molecules are centrosymmetric with inversion centers located at the middle of the central N═N (**2**), C−C (**3**), and C═C (**4**) bonds between the pyridyl rings. The bridging bpa ligand in **1** adopts the *anti* conformation, its pyridyl rings being parallel with an interplanar distance of 1.344(1) Å.

$\{[Mn(Etmal)_2(H_2O)][Mn(H_2O)_4]\}_n$ (***5***). Compound **5** crystallizes in the chiral space group $C222_1$ and its structure consists of neutral zigzag chains with a regular alternation of $[Mn(Etmal)_2(H_2O)]^{2-}$ anions and $[Mn(H_2O)_4]^{2+}$ cations which are linked through *anti-syn* carboxylate bridges and that grow along the crystallographic *c* axis (Figures 5 and 6).

Two crystalographically different manganese(II) ions [Mn(1) and Mn(2)] are present in **5**. The Mn(1) atom is five-coordinated in a trigonal bipyramidal environment with a τ value of 0.96 (τ being 0 for a square pyramidal and 1 for a trigonal bipyramidal environment):[18] two oxygen atoms from two different ethylmalonate ligands [O(2) and O(2e); symmetry code: (e) = $-x$, y, $1/2-z$] and a coordinated water molecule [O(1W)] build the trigonal equatorial plane [average value for the Mn(1)−O(eq) bond lengths is 2.0910(13) Å] whereas the axial positions are filled by two oxygen atoms [O(4) and O(4e)] from two symmetry-related Etmal ligands [mean value for the Mn(1)−O(ax) bond distances being 2.1150(9) Å]. The Mn(2) atom from the $[Mn(H_2O)_4]$ unit is six-coordinated in a distorted octahedral environment, the values of the *s*/*h* and ϕ parameters being 1.26 and 58.16°, respectively. The equatorial plane at Mn(2) is defined by four water molecules [O(2W), O(2Wf), O(3W), and O(3Wf); symmetry code: (f) = x, $-y$, $1-z$] whereas the axial positions are occupied by two oxygen atoms [O(1) and

dx.doi.org/10.1021/ic201314k |*Inorg. Chem.* 2011, 50, 10765–10776

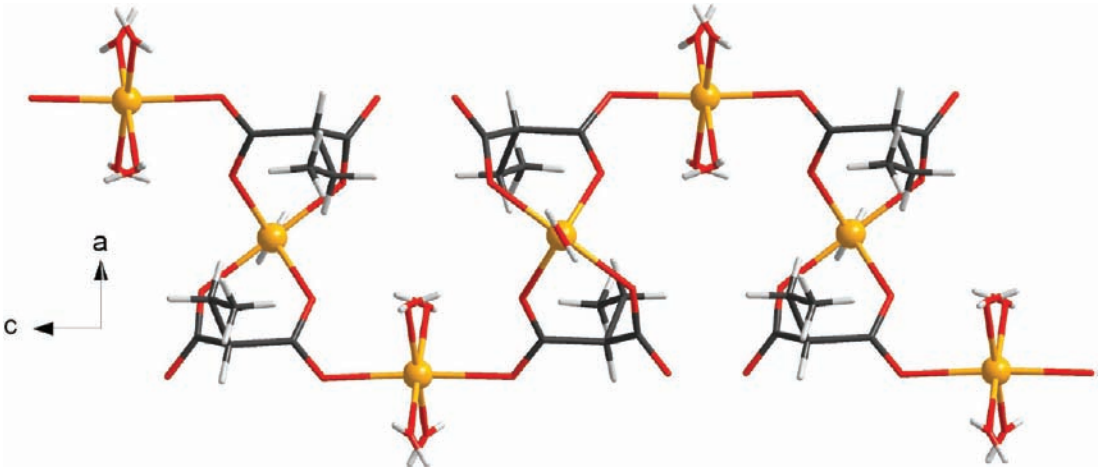

Figure 6. View along the crystallographic *b* axis of a carboxylate-bridged Mn(II) chain of **5** showing the regular alternation manganese(II) ions in trigonal bipyramidal and octahedral environments.

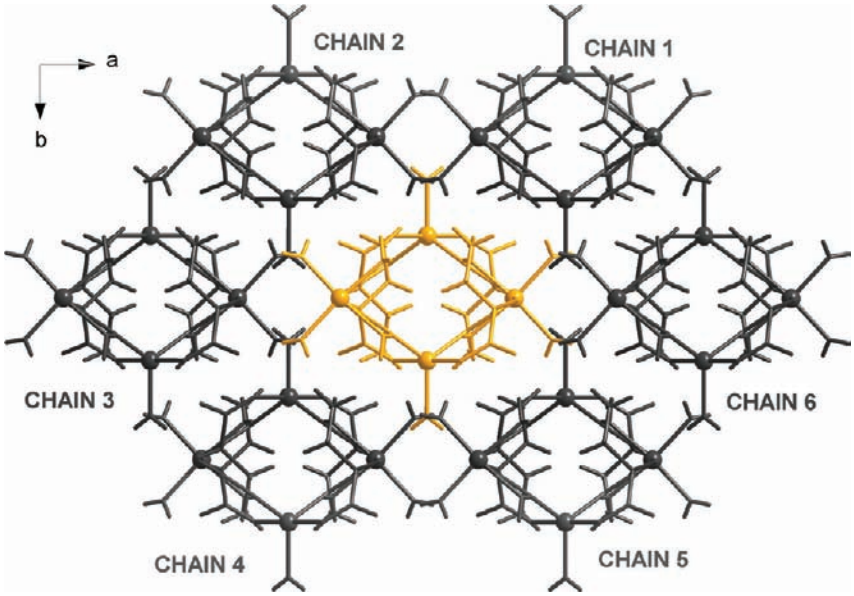

Figure 7. Perspective view of the crystal packing in **5** along the crystallographic *c* axis showing all the symmetry-related chains (black color) around the central one (yellow color).

O(1f)] from two different Etmal ligands. The values of the average Mn(2)−O(eq) and Mn(2)−O(ax) bond distances are 2.1510(11) and 2.2680(7) Å, respectively.

The $[Mn(Etmal)_2(H_2O)]$ unit is chiral, and it adopts either the Δ or the Λ enantiomeric conformation within each chain. Then, regular alternation of chains containing only one enantiomeric form occurs in **5**. A given chain in **5** is surrounded by other six ones in a close crystal packing, this structural feature precluding the presence of crystallization water molecules (Figure 7). The chains are linked through hydrogen bonds between the coordinated water molecules and the coordinated and uncoordinated ethylmalonate oxygen atoms to build a supramolecular 3D network [mean O···O distance being 2.745(2) Å; see Table 5]. The hydrogen bonding pattern for the two repeating units along the chain is shown in Figure 8. One can see there how the $[Mn(Etmal)_2(H_2O)]$ units are interconnected to six adjacent chains while the tetraaquamanganese(II) units are linked to three of them.

The crystallographically independent ethylmalonate ligand acts simultaneously as bidentate [through O(4) and O(2) toward Mn(1), the angle subtended at the manganese atom being 86.22(3)°] and monodentate [through O(1) toward Mn(2)]. The bidentate coordination of the Etmal ligand involves one equatorial [O(2e)] and one axial position [O(4e)] of Mn(1), this manganese center becoming stereogenic in the resulting above-described trigonal bipyramidal environment. Regular alternating Mn(1) and Mn(2) atoms occurs within each chain with a carboxylate-ethyl malonate group in the *anti-syn* conformation acting as the intrachain bridge and connecting one equatorial position of Mn(1) to an axial one at Mn(2). The intrachain Mn(1)···Mn(2) separation is 5.3167(4) Å, a value which is slightly shorter than the shortest interchain metal−metal separation

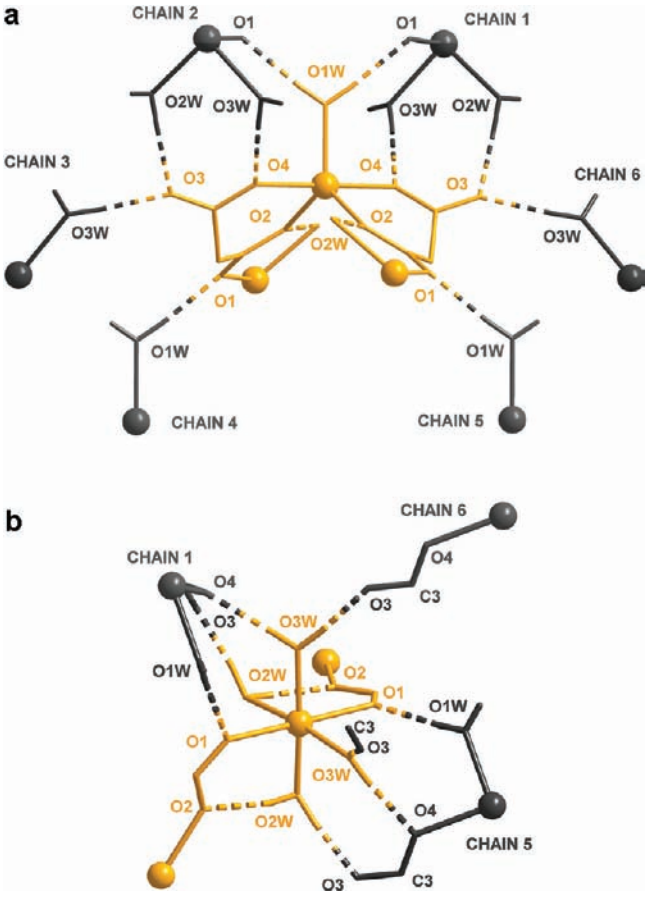

Figure 8. Hydrogen bonding around the $[Mn(Etmal)_2(H_2O)]^{2-}$ (a) and $[Mn(H_2O)_4]^{2+}$ (b) units in **5**.

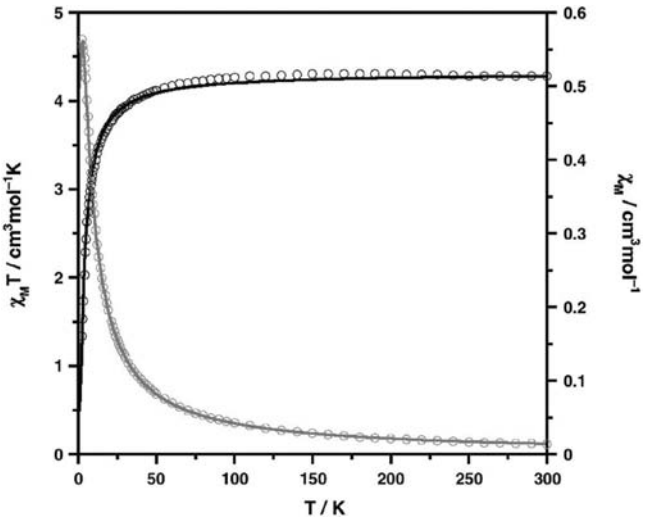

Figure 9. $\chi_M T$ (black) and χ_M (gray) vs T plots for compound **1**. The solid line is the best-fit curve (see text).

[Mn(1 g)···Mn(2) = 5.4344(5) Å; symmetry code: (g) = $-x+1/2$, $-y+1/2$, $z+1/2$]. This close intermolecular connection between Mn(1) and Mn(2) occurs through two different hydrogen bonds [Mn(2)−O(3W)···O(4)−Mn(1) and Mn(2)−O(1)···O(1W)−Mn(1)].

Thermal Study. Complexes **1** and **2** [Supporting Information, Figure S1 (a) and (b)] exhibit a fast decomposition transforming into MnO (found and calculated weight loss are 29.0 and 24.0% for **1** and 29.9 and 24% for **2**, respectively) from 180 (**1**) and 195 °C (**2**). Complex **3** and **4** [Supporting Information, Figure S1 (c) and (d)] presents slightly progressive weight loss from room temperature to 210 (**3**) and 190 °C (**4**) which corresponds to the release of the coordinated water molecule [found/calculated weight loss of 6.10/6.40% (**3**) and 6.9/6.12% (**4**)]. The resulting anhydrous phases are not stable, and they undergo a fast decomposition transforming into MnO (found/calculated weight loss are 19.91/25.0% (**3**) and 16.0/24.0% (**4**)].

In the case of compound **5**, it is stable until 120 °C. At greater temperatures, the thermogravimetric analysis (TGA) data show two successive weight losses [see Supporting Information, Figure S1 (d)]. The first one corresponds to the full dehydration [found/calculated weight loss for the five water molecules of 19.0/19.28%]. The resulting anhydrous phase is stable until 250 °C, and it further decomposes to yield Mn_2O_3 [found/calculated weight loss of 34.53/34.31%].

Magnetic Properties. Variable-temperature magnetization measurements were performed on powdered polycrystalline samples of **1**−**5** under applied direct current (dc) magnetic fields of 1 T ($30 \le T \le 300$ K) and 0.1 T ($1.9 \le T \le 30$ K). The results under the form of both $\chi_M T$ and χ_M versus T plots [χ_M being the magnetic susceptibility per one manganese(II) ion] are shown in Figures 9 (**1**), 10 (**5**), and Supporting Information, Figures S2 (**2**), S3 (**3**), and S4 (**4**), respectively. At room temperature, $\chi_M T$ is equal to 4.28 (**1**), 4.31 (**2**), 4.29 (**3**), 4.28 (**4**), and 4.38 cm^3 mol^{-1} K (**5**). These values correspond to that expected for an magnetically isolated manganese(II) ion ($\chi_M T$ = 4.375 cm^3 mol^{-1} K for $S_{Mn} = 5/2$ and $g = 2.0$). Upon cooling, the values of $\chi_M T$ remain practically constant until T about 120 K, and they decrease monotonically at lower temperatures to reach minimum values of 1.35 (**1**), 0.70 (**2**), 0.74 (**3**), 0.71 (**4**), and 1.75 cm^3 mol^{-1} K (**5**) at 1.9 K. These plots are characteristic of an overall weak antiferromagnetic coupling in **1**−**5**, which in the case of three of them (**2**−**4**) is supported by the presence of a maximum of the magnetic susceptibility at 3.4 (**2**), 3.9 (**3**), and 3.3 K (**4**).

On the basis of the crystal structure of the complexes **1**−**4**, two exchange pathways could be involved: the carboxylate-bridge in the *anti-syn* conformation and the extended bis-monodentate N-donors. The much larger values of manganese−manganese separation through the latter pathway (values in the range 11.7−13.9 Å) when compared with those across the former one (values in the range 5.4−5.5 Å) together with the known ability of the carboxylate bridge to mediate magnetic interactions,[3g,19] allow us to conclude that the magnetic properties of **1**−**4** would correspond to those of an alternating square-grid system. In this context, an unique magnetic coupling (J_1) would be responsible to the alignment of the magnetic centers along a direction in the plane, whereas another one (J_2) would operate in the orthogonal direction.

Prior to the analysis of the magnetic data of **1**−**4**, we would like to present some considerations about the best methodology to be used. The simulation of the magnetic properties is an important step for a correct analysis of the magnetic exchange in polynuclear compounds such as **1**−**4**. Procedures based on the exact energy matrix diagonalization are commonly used to do this task but their applicability is limited by the size of the systems, in particular in the case of the extended ones. Monte Carlo methods

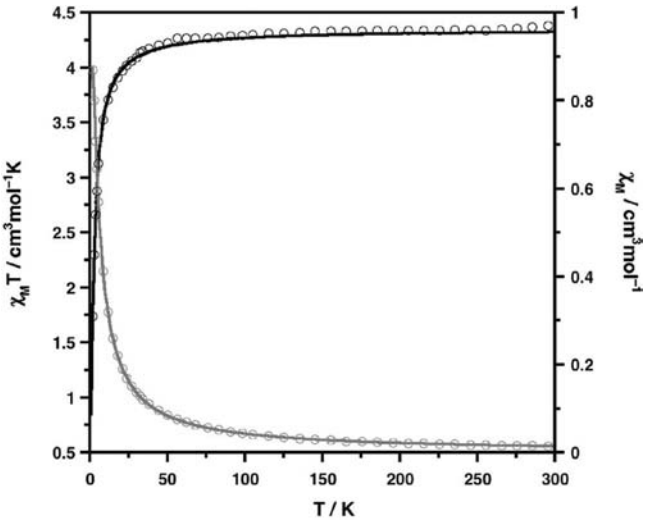

Figure 10. $\chi_M T$ (black) and χ_M (gray) vs T plots for compound **5**. The solid line is the best-fit curve (see text).

are well suited to analyze these latter systems, and they are among the most used ones for that purpose.[20−22] On the other hand, the use of a classical spin law can be a good option to simulate the magnetic behavior of these extended systems with large local spin moments.[23] In a review published by one of us, it was proved that these available classical laws for 2D and 3D systems are not suitable.[24] In such a review, results from Monte Carlo,[24] spin-path progressive addition,[24] high-temperature series expansions methods,[25−27] and known laws[28,29] for the mentioned networks were compared. Only the last ones provide simulations that disagree with those given by other methods, and even the best-fit values of the magnetic coupling obtained by the analysis of experimental data using these laws differ from those determined in similar but simpler systems such as dinuclear compounds. That is why we have decided to propose a new empirical law derived from Monte Carlo (MC) simulations based on the classical spin approach. These simulations were done on a 40 × 40 model where periodic boundary conditions have been introduced to be close to the physical behavior of a two-dimensional network. The number of the Monte Carlo steps by site was 5×10^5. The first 5×10^4 generated configurations were discarded at each temperature because they were associated with the thermalization process. At this point, it was considered that the equilibrium was reached, and the magnetic susceptibility and the $\chi_M T$ product of each spin configuration generated by the Metropolis algorithm were registered to evaluate the average values of these physical properties. The $\chi_M T$ product was obtained from the fluctuations in the magnetization through eq 1, where $\langle M \rangle$ and $\langle M^2 \rangle$ are the mean values of magnetization and its square, and N, β, and k have their usual meaning.

$$\chi_M T = \frac{N\beta^2}{k}(\langle M^2 \rangle - \langle M \rangle^2) \quad (1)$$

To avoid the spin configurations to be frozen because of a fast cooling of the sample, a low cooling rate is chosen (starting from a high temperature) according to the following expression [eq 2]:

$$T_{i+1} = 0.95 T_i \quad (2)$$

Thus, the points at low temperature, where the relaxation time is large, become closer. As mentioned above, we used the Metropolis algorithm to accept or to discard a new proposed spin configuration in each MC step in agreement with a Boltzmann distribution.[30] More detailed information can be found in some of our previous publications.[24,31,32] Finally, the collected data were handled to find an empirical law that was able to reproduce accurately the original data. To make this procedure easier, we worked with reduced variables ($\chi_M J$ and T/J). Thus, when only a magnetic coupling (J) is present, only one curve is needed to reproduce the magnetic behavior of a system independently on the strength of the magnetic coupling. In **1**−**4**, where two different magnetic couplings coexist, a series of curves that are dependent on the α parameter (that is the ratio between the magnetic couplings, J_2/J_1) are required. In our case, whereas J_2 can be ferromagnetic (positive values) or antiferromagnetic (negative values), J_1 only corresponds to an antiferromagnetic coupling. Because the antiferromagnetic coupling is predominant in **1**−**4**, α can take values in the range −1 to +1, that is, J_1 is ever stronger than J_2 ($|J_1| \geq |J_2|$). The inclusion of the $S(S+1)$ term in the reduced variable [$\chi_M J$ and $T/JS(S+1)$] leads to the universal use of the empirical law for any value of the local spin moment (S). So, the simulated curves were used to deduce an empirical law which is derived by minimizing a quotient between two polynomials and that takes the following expression [eq 3]:

$$\chi_M J = \frac{1}{4} g^2 \frac{\sum_{i=0}^{3} \left(\sum_{j=0}^{4} A_{i,j} \alpha^j \right) T_r^i}{\sum_{i=0}^{4} \left(\sum_{j=0}^{4} B_{i,j} \alpha^j \right) T_r^i} \quad (3)$$

In this expression, T_r is the reduced temperature expressed as $T/JS(S+1)$ and g and S are the Landé factor and the spin of the paramagnetic center, respectively. The corresponding coefficients are listed in Table 6. Even in a general formulation, this empirical law is not valid for low reduced temperatures. So, for smaller and larger $|\alpha|$ values, the empirical law can only be used for $T_r \geq 0.2$ and 0.5, respectively. This limitation is only related

Table 6. Coefficients for the Empirical Law Used to Reproduce the Dependence of the Magnetic Susceptibility on the Temperature, the Strength of the Magnetic Couplings, and the Local Spin Moment of an Alternated Square 2D Network[a,b]

i	j	$A_{i,j,k}$	$B_{i,j,k}$	i	j	$A_{i,j,k}$	$B_{i,j,k}$
0	0	0.559825	3.816090	2	3	13.984072	−297.87661
0	1	0.452442	1.925866	2	4	−482.58713	614.965534
0	2	305.14904	1519.98664	3	0	748.285843	1015.79002
0	3	−10.762452	475.450309	3	1	−23.815104	1251.13315
0	4	−7.165649	551.146212	3	2	−9.942938	206.795962
1	0	98.322841	371.505560	3	3	−234.76575	−42.250799
1	1	12.765276	270.624214	3	4	235.797869	−1138.2458
1	2	−722.85868	−2780.5442	4	0		1499.74539
1	3	−35.417235	−758.41818	4	1		−60.231547
1	4	360.118072	−421.18559	4	2		−16.870338
2	0	6.309606	422.677481	4	3		−459.57473
2	1	127.834552	127.25602	4	4		505.369724
2	2	297.281336	1178.11151				

[a] The expression and limitations of this law are given in the text. [b] It is important to notice these coefficients are valid when the value of the J_1 parameter is given in K.

to our simulations and to the size of the model used in them and not to the classical spin approach. Thus, the applicability range will be strongly reduced for very small local spin moments ($S \leq 3/2$) because of the inclusion of the quantum effects, but the use of this approach is not allowed in such cases.

This empirical law was used to estimate the parameters charged on the description of the magnetic behavior of **1**−**4**. The best-fit curves (see Figure 9 and Supporting Information, Figures S2−S4) were obtained with the following parameters: $g = 1.990 \pm 0.005$, $J_1 = -0.354 \pm 0.010$ cm^{-1}, $J_2 = +0.03 \pm 0.06$ cm^{-1} and $R = 1.9 \times 10^{-4}$ for **1**, $g = 2.000 \pm 0.005$, $J_1 = -0.377 \pm 0.010$ cm^{-1}, $J_2 = -0.18 \pm 0.03$ cm^{-1} and $R = 3.6 \times 10^{-5}$ for **2**, $g = 1.998 \pm 0.003$, $J_1 = -0.433 \pm 0.006$ cm^{-1}, $J_2 = -0.17 \pm 0.04$ cm^{-1} and $R = 5.2 \times 10^{-5}$ for **3**, and $g = 1.990 \pm 0.003$, $J_1 = -0.36 \pm 0.03$ cm^{-1}, $J_2 = -0.186 \pm 0.007$ cm^{-1} and $R = 5.4 \times 10^{-5}$ for **4** (R is the agreement factor defined as $\Sigma_i[(\chi_M)_{obs}(i) - (\chi_M)_{calc}(i)]^2/\Sigma_i[(\chi_M)_{obs}(i)]^2$). The calculated curves reproduce well the experimental data in the whole temperature range investigated.

Dealing with compound **5**, we are faced to a uniform chain compound of interacting spin sextuplets, the intrachain magnetic coupling being weak and antiferromagnetic. Therefore, its magnetic data can be analyzed by means of Fischer's law for a regular chain with classical spin moments or with our empirical law where $\alpha = 0$ is imposed. It is quite satisfying to note that the same results were reached through both models. The best-fit parameters are $g = 2.0007 \pm 0.0009$, $J_1 = -0.2207 \pm 0.0018$ cm^{-1}, and $R = 5.7 \times 10^{-6}$.

The weak antiferromagnetic couplings and occasionally very weak ferromagnetic couplings obtained by fit in **1**−**5** are in agreement with the expected interactions between manganese(II) ions through a single carboxylate in the *syn-anti* coordination mode, the somewhat greater magnitude in **1**−**4** versus **5** being because the carboxylate links equatorial positions of adjacent metal atoms in the former whereas it connects an equatorial with an axial position in the latter one.

CONCLUSIONS

The introduction of the rod-like N-donor bpe, azpy, 4,4′-bpy, and bpa as coligands in the ethylmalonate-manganese(II) system allowed us to transform the chain compound **5** into the 3D networks **1**−**4** where corrugated quasi square grids of carboxylate-bridged manganese(II) ions are interconnected through the extended bis-monodentate nitrogen donors. The fact that the coligands and the manganese(II) ethylmalonate layers are not perpendicular to each other together with the interlayer positions of the ethyl groups of the ethylmalonate ligand leaves practically no void space between the layers avoiding the formation of cavities or pores. This structural feature has been also found in the related compounds $[Mn_2(mal)_2(H_2O)_2(4,4'\text{-bpy})]_n$[3g] and $[Cu_2(Memal)_2(H_2O)_2(4,4'\text{-bpy})]_n$[6d] ($H_2$mal = malonic acid and H_2Memal = methylmalonic acid), and curiously no significant structural modifications can be observed despite of the different alkyl-substituted malonates used. The magnetic properties of this kind of complexes are a priori interesting because they are 3D polynuclear complexes involving high-spin centers. Although similar structures quoted before[24] present weak antiferromagnetic interactions along the *anti-syn* carboxylate bridges, the use of other transition metals ions to prepare homo- or heterometallic species would result in an overall ferro- or ferrimagnetic behaviors. Remarkably, the anhydrous phase of complex **5** does not decompose until 250 °C, while those of complexes **1**−**4** are not stable, and they undergo a fast decomposition at around 200 °C.

ASSOCIATED CONTENT

Supporting Information. Additional details are given in Figures S1 (TG/DTG/DTA plots for **1**−**4**) and S2−S4 (magnetic plots for **2**−**4**). Crystallographic data are provided in CIF format. This material is available free of charge via the Internet at http://pubs.acs.org.

AUTHOR INFORMATION

Corresponding Author

*E-mail: jpasang@ull.es (J.P.), caruiz@ull.es (C.R.-P.).

Present Addresses

⊥Instituto de Ciencia de Materiales de Aragón, CSIC-Universidad de Zaragoza, C/Pedro Cerbuna 12, E-50009, Zaragoza, Spain and Institut Laue-Langevin, Grenoble, rue Jules Horowitz, B.P. 156, 38042 Grenoble Cedex 9, France.

ACKNOWLEDGMENT

Financial support by the Spanish Ministerio de Ciencia e Innovación through projects MAT2007-60660, MAT2010-16981, CTQ2010-15364, DPI2010-21103-C04-03, "Factoría de Crystalización" (Consolider Ingenio2010 CSD2006-0015), Molecular Nanoscience (Consolider Ingenio CSD2007-00010), ACIISI Gobierno de Canarias and Generalitat Valenciana (PROMETEO/2009/108) is gratefully acknowledged. M.D. and J.F.-S. thank the Spanish Ministerio de Ciencia e Innovación (M.D.) and the Generalitat Valenciana (J.F.-S.) for predoctoral fellowships. J.P. also thanks the Proyecto Estructurante NANOMAC (ACIISI-Gobierno de Canarias) for a postdoctoral contract.

REFERENCES

(1) Rao, C. N. R.; Natarajan, S.; Vaidhyanathan, R. *Angew. Chem., Int. Ed.* **2004**, *43*, 1466.

(2) Hernández-Molina, M.; Lorenzo-Luis, P. A.; Ruiz-Pérez, C. *CrystEngComm* **2001**, *3*, 60.

(3) (a) Bimitrova, G. I.; Ablov, A. V.; Popovich, G. A.; Nmalinouskii, T. I.; Bourshteyn, I. F. *Dokl. Akad. Nauk SSSR* **1974**, *216*, 1055. (b) Rodríguez-Martín, Y.; Sanchiz, J.; Ruiz-Pérez, C.; Lloret, F.; Julve, M. *CrystEngComm* **2002**, *4*, 631. (c) Chattopadhyay, D.; Chattopadhyay, S. K.; Lowe, P. R.; Schwalbe, C. H.; Mazumdar, S. K.; Rana, A.; Ghosh, S. *J. Chem. Soc., Dalton Trans.* **1993**, 913. (d) Ruiz-Pérez, C.; Sanchiz, J.; Hernández-Molina, M.; Lloret, F.; Julve, M. *Inorg. Chem.* **2000**, *39*, 1363. (e) Hornick, C.; P. Rabu, P.; M. Drillon, M. *Polyhedron* **2000**, *19*, 259. (f) Rabu, P.; Rueff, J. M.; Huang, Z. L.; Angelov, S.; Souletie, J.; Drillon, M. *Polyhedron* **2001**, *20*, 1677. (g) Rodríguez-Martín, Y.; Hernández-Molina, M.; Sanchiz, J.; Ruiz-Pérez, C.; Lloret, F.; Julve, M. *Dalton Trans.* **2003**, 2359–2365.

(4) (a) Gable, R. W.; Hoskins, B. F.; Robson, R. *J. Chem. Soc., Chem. Commun.* **1990**, 1677. (b) Carlucci, L.; Ciani, G.; Proserpio, D. M.; Sironi, A. *Inorg. Chem.* **1995**, *34*, 5698. (c) Subramanian, S.; Zaworotko, M. J. *Angew. Chem., Int. Ed. Engl.* **1995**, *34*, 2127. (d) Lloret, F.; De Munno, G.; Julve, M.; Cano, J.; Ruiz, R.; Caneschi, A. *Angew. Chem., Int. Ed.* **1998**, *37*, 135. (e) Blake, A. J.; Champness, N. R.; Crew, M.; Hanton, L. R.; Parsons, S.; Schröder, M. *J. Chem. Soc., Dalton Trans.* **1998**, 1533.

(5) Rodríguez-Martín, Y.; Ruiz-Pérez, C.; Sanchiz, J.; Lloret, F.; Julve, M. *Inorg. Chim. Acta* **2001**, *318*, 159.

(6) Methylmalonate-containing complexes: (a) Déniz, M.; Pasán, J.; Fabelo, O.; Cañadillas-Delgado, L.; Lloret, F.; Julve, M.; Ruiz-Pérez, C. *New J. Chem.* **2010**, *34*, 2515. (b) Pasán, J.; Sanchiz, J.; Cañadillas-Delgado, L.; Fabelo, O.; Déniz, M.; Lloret, F.; Julve, M.; Ruiz-Pérez, C. *Polyhedron* **2009**, *28*, 1802. (c) Gkioni, C.; Boudalis, A. K.; Sanakis, Y.; Raptopoulou, C. P. *Polyhedron* **2007**, *26*, 2536. (d) Pasán, J.; Sanchiz, J.; Lloret, F.; Julve, M.; Ruiz-Pérez, C. *CrystEngComm* **2007**, *9*, 478. (e) Perkins, C. M.; Rose, N. J.; Stenkamp, R. E. *Inorg. Chim. Acta* **1990**, *172*, 119.

(7) Phenylmalonate-containing complexes: (a) Pasán, J.; Sanchiz, J.; Ruiz-Pérez, C.; Campo, J.; Lloret, F.; Julve, M. *Polyhedron*, manuscript accepted for publication. (b) Pasán, J.; Sanchiz, J.; Ruiz-Pérez, C.; Campo, J.; Lloret, F.; Julve, M. *Chem. Commun.* **2006**, 2857. (c) Pasán, J.; Sanchiz, J.; Ruiz-Pérez, C.; Lloret, F.; Julve, M. *Inorg. Chem.* **2005**, *44*, 7794. (d) Pasán, J.; Sanchiz, J.; Ruiz-Pérez, C.; Lloret, F.; Julve, M. *Eur. J. Inorg. Chem.* **2004**, 4081. (e) Pasán, J.; Sanchiz, J.; Ruiz-Pérez, C.; Lloret, F.; Julve, M. *New J. Chem.* **2003**, *27*, 1557.

(8) (a) Brown, E. V.; Granneman, G. R. *J. Am. Chem, Soc.* **1975**, *97*, 621. (b) Kirpal., A.; Reiter., E. *Chem. Ber.* **1927**, *60*, 664. (c) Kirpal, A. *Chem. Ber.* **1934**, *67*, 70. (d) Launay, J. P.; Tourrel-Pagois, M.; Lipskier, J. F.; Marvaud, V.; Joachim., C. *Inorg. Chem.* **1991**, *30*, 1033.

(9) Carlin, R. L. *Magnetochemistry*; Springer-Verlag: Berlin, Germany, 1986.

(10) Otwinowski, Z.; Minor, M. *Macromolecular Crystallography, A, Methods in Enzymology*; Academic Press: New York, 1997; pp 276, 307−326.

(11) Sheldrick, G. M. *SHELXL-97, SHELXS-97, Programs for Crystal Structure Refinement*; Universität Göttingen: Göttingen, Germany, 1998.

(12) Farrugia, J. L. *J. Appl. Crystallogr.* **1999**, *32*, 837.

(13) Nardelli, M. *J. Appl. Crystallogr.* **1995**, *28*, 659.

(14) *DIAMOND 2.1d*; Crystal Impact GbR, K. Brandenburg & H. Putz GbR: Bonn, Germany, 2000.

(15) Janiak, C. *Dalton Trans.* **2000**, 3885.

(16) Hirota, H.; Sakaibara, K.; Suezawa, H.; Yuzuri, T.; Ankai, E.; Nishio, M. *J. Phys. Org. Chem.* **2000**, *13*, 620–623.

(17) Stiefel, E. I.; Brown, G. F. *Inorg. Chem.* **1972**, *11*, 434.

(18) Addison, A. W.; Rao, T. N.; Reedijk, J.; van Rijn, J.; Verschoor, G. C. *Dalton Trans.* **1984**, 1349.

(19) Rodríguez-Fortea, A.; Alemany, P.; Alvarez, S.; Ruiz, E. *Chem. —Eur. J.* **2001**, *7*, 627, and references therein.

(20) Suzuki, M. In *Quantum Monte Carlo Methods in Condensed Matter Physics*; M. Suzuki, M., Ed.; World Scientific Publishing Co. Pte. Ltd.: Singapore, 1993; pp 163−177.

(21) Binder, K.; K.; Heermann, D. W. In *Monte Carlo Simulation in Statistical Physics. An Introduction*; Fulde, P., Ed.; Springer Series in Solid State Sciences, 3rd ed.; Springer: Berlin, Germany, 1997.

(22) Landau, D. P.; Binder, K. In *A Guide to Monte Carlo Simulations in Statistical Physics*, 3rd ed.; Cambridge University Press: Cambridge, U.K., 2009.

(23) Fisher, M. E. *Am. J. Phys.* **1964**, *32*, 343.

(24) Cano, J.; Journaux, Y. In *Magnetism: Molecules to Materials V*; Miller, J. S., Drillon, M., Eds.; Wiley-VCH: Weinheim, Germany, 2005; pp 189−222.

(25) Navarro, R. In *Magnetic Properties of Layered Transition Metal Compounds*; Jongh, L. J. D., Ed.; Kluwer Academic Publishers: Dordrecht, The Netherlands, 1990; p 105.

(26) Camp, W. L.; Dye, J. P. V. *J. Phys. (Paris)* **1975**, *C8*, 336.

(27) Stanley, H. E. *Phys. Rev.* **1967**, *158*, 456.

(28) Curély, J.; Lloret, F.; Julve, M. *Phys. Rev. B* **1998**, *58*, 11456.

(29) Curély, J. *Europhys. Lett.* **1995**, *32*, 529.

(30) Metropolis, N.; Rosenbluth, A. W.; Rosenbluth, M. N.; Teller, A. H.; Teller, E. *J. Chem. Phys.* **1953**, *21*, 1087.

(31) Boullant, E.; Cano, J.; Journaux, Y.; Decurtins, S.; Gross, M.; Pilkington, M. *Inorg. Chem.* **2001**, *16*, 3900.

(32) Cañadillas-Delgado, L.; Fabelo, O.; Cano, J.; Pasán, J.; Delgado, F. S.; Lloret, F.; Julve, M.; Ruiz-Pérez, C. *CrystEngComm* **2009**, *11*, 2131.